















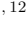









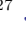
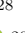






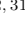

















VENUS:
Two Faint Little Red Dots Separated by ~ 70 pc
Hidden in a Single Lensed Galaxy at $z \sim 7$

HIROTO YANAGISAWA ^{1,2} MASAMI OUCHI ^{3,1,4,5} MIRIAM GOLUBCHIK ⁶ MASAMUNE OGURI ^{7,8}
SEIJI FUJIMOTO ^{9,10} VASILY KOKOREV ^{11,12} GABRIEL BRAMMER ^{13,14} FENGWU SUN ¹⁵ MINAMI NAKANE ^{1,2}
YUICHI HARIKANE ¹ HIROYA UMEDA ^{1,2} HOLLIS B. AKINS ¹¹ HAKIM ATEK ¹⁶ FRANZ E. BAUER ¹⁷
MARUŠA BRADAČ ^{18,19} JOHN CHISHOLM ^{11,12} DAN COE ^{20,21,22} JOSE M. DIEGO ²³ HENRY C. FERGUSON ²⁰
STEVEN L. FINKELSTEIN ^{11,12} LUKAS J. FURTAK ^{11,12} KOHEI INAYOSHI ²⁴ ANTON M. KOEKEMOER ²⁰
JORRYT MATTHEE ²⁵ ROHAN P. NAIDU ²⁶ YOSHIAKI ONO ¹ RICHARD PAN ²⁷ JOHAN RICHARD ²⁸
LUKE ROBBINS ²⁷ CHRIS WILLOTT ²⁹ ADI ZITRIN ⁶ RICARDO O. AMORÍN ³⁰ LARRY D. BRADLEY ²⁰
VOLKER BROMM ^{11,12,31} CHRISTOPHER J. CONSELICE ³² PRATIKA DAYAL ^{33,9,34} JEYHAN S. KARTALTEPE ³⁵
PAULO A. A. LOPES ³⁶ RAY A. LUCAS ²⁰ GEORGIOS E. MAGDIS ^{13,37} NICHOLAS S. MARTIS ¹⁸
CASEY PAPOVICH ^{38,39} DANIEL SCHAEERER ⁴⁰ FRANCESCO VALENTINO ^{13,37} EROS VANZELLA ⁴¹
JOSEPH F. V. ALLINGHAM ⁶ NORMAN A. GROGIN ²⁰ MAURO GONZÁLEZ-OTERO ⁴² MASSIMO RICOTTI ⁴³ AND
ROGIER A. WINDHORST ⁴⁴

¹*Institute for Cosmic Ray Research, The University of Tokyo, 5-1-5 Kashiwanoha, Kashiwa, Chiba 277-8582, Japan*

²*Department of Physics, Graduate School of Science, The University of Tokyo, 7-3-1 Hongo, Bunkyo, Tokyo 113-0033, Japan*

³*National Astronomical Observatory of Japan, 2-21-1 Osawa, Mitaka, Tokyo 181-8588, Japan*

⁴*Department of Astronomical Science, SOKENDAI (The Graduate University for Advanced Studies), 2-21-1 Osawa, Mitaka, Tokyo, 181-8588, Japan*

⁵*Kavli Institute for the Physics and Mathematics of the Universe (WPI), The University of Tokyo, 5-1-5 Kashiwanoha, Kashiwa, Chiba 277-8583, Japan*

⁶*Department of Physics, Ben-Gurion University of the Negev, P.O. Box 653, Beer-Sheva 8410501, Israel*

⁷*Center for Frontier Science, Chiba University, 1-33 Yayoi-cho, Inage-ku, Chiba 263-8522, Japan*

⁸*Department of Physics, Graduate School of Science, Chiba University, 1-33 Yayoi-Cho, Inage-Ku, Chiba 263-8522, Japan*

⁹*David A. Dunlap Department of Astronomy and Astrophysics, University of Toronto, 50 St. George Street, Toronto, Ontario, M5S 3H4, Canada*

¹⁰*Dunlap Institute for Astronomy and Astrophysics, 50 St. George Street, Toronto, Ontario, M5S 3H4, Canada*

¹¹*Department of Astronomy, The University of Texas at Austin, 2515 Speedway Blvd Stop C1400, Austin, TX 78712, USA*

¹²*Cosmic Frontier Center, The University of Texas at Austin, Austin, TX 78712, USA*

¹³*Cosmic Dawn Center (DAWN), Jagtvej 128, DK2200 Copenhagen N, Denmark*

¹⁴*Niels Bohr Institute, University of Copenhagen, Jagtvej 128, 2200 Copenhagen N, Denmark*

¹⁵*Center for Astrophysics | Harvard & Smithsonian, 60 Garden St., Cambridge, MA 02138, USA*

¹⁶*Institut d'Astrophysique de Paris, CNRS, Sorbonne Université, 98bis Boulevard Arago, 75014, Paris, France*

¹⁷*Instituto de Alta Investigación, Universidad de Tarapacá, Casilla 7D, Arica, 1010000, Chile*

¹⁸*University of Ljubljana, Faculty of Mathematics and Physics, Jadranska ulica 19, SI-1000 Ljubljana, Slovenia*

¹⁹*Department of Physics and Astronomy, University of California Davis, 1 Shields Avenue, Davis, CA 95616, USA*

²⁰*Space Telescope Science Institute, 3700 San Martin Drive, Baltimore, MD 21218, USA*

²¹*Association of Universities for Research in Astronomy (AURA), Inc. for the European Space Agency (ESA)*

²²*Center for Astrophysical Sciences, Department of Physics and Astronomy, The Johns Hopkins University, 3400 N Charles St. Baltimore, MD 21218, USA*

²³*Instituto e Física de Cantabria, (CSIC-UC), Avda. Los Castros s/n. 39005, Santander, Spain*

²⁴*Kavli Institute for Astronomy and Astrophysics, Peking University, Beijing 100871, China*

²⁵*Institute of Science and Technology Austria (ISTA), Am Campus 1, 3400 Klosterneuburg, Austria*

²⁶*MIT Kavli Institute for Astrophysics and Space Research, 70 Vassar Street, Cambridge, MA 02139, USA*

²⁷*Department of Physics and Astronomy, Tufts University, 574 Boston Avenue, Suite 304, Medford, MA 02155, USA*

²⁸*Univ Lyon, Univ Lyon1, ENS de Lyon, CNRS, Centre de Recherche Astrophysique de Lyon UMR5574, 69230 Saint-Genis-Laval, France*

²⁹*NRC Herzberg, 5071 West Saanich Rd, Victoria, BC V9E 2E7, Canada*

³⁰*Instituto de Astrofísica de Andalucía (CSIC), Apartado 3004, 18080 Granada, Spain*

³¹Weinberg Institute for Theoretical Physics, University of Texas, Austin, TX 78712, USA

³²Jodrell Bank Centre for Astrophysics, University of Manchester, Oxford Road, Manchester M13 9PL, UK

³³Canadian Institute for Theoretical Astrophysics, 60 St George St, University of Toronto, Toronto, ON M5S 3H8, Canada

³⁴Department of Physics, 60 St George St, University of Toronto, Toronto, ON M5S 3H8, Canada

³⁵Laboratory for Multiwavelength Astrophysics, School of Physics and Astronomy, Rochester Institute of Technology, 84 Lomb Memorial Drive, Rochester, NY 14623, USA

³⁶Observatório do Valongo, Universidade Federal do Rio de Janeiro, Ladeira do Pedro Antônio 43, Rio de Janeiro, RJ, 20080-090, Brazil

³⁷DTU-Space, Technical University of Denmark, Elektrovej 327, 2800, Kgs. Lyngby, Denmark

³⁸Department of Physics and Astronomy, Texas A&M University, College Station, TX 77843-4242, USA

³⁹George P. and Cynthia Woods Mitchell Institute for Fundamental Physics and Astronomy, Texas A&M University, College Station, TX 77843-4242, USA

⁴⁰Department of Astronomy, University of Geneva, Chemin Pegasi 51, 1290 Versoix, Switzerland

⁴¹INAF – OAS, Osservatorio di Astrofisica e Scienza dello Spazio di Bologna, via Gobetti 93/3, I-40129 Bologna, Italy

⁴²Instituto de Astrofísica de Andalucía–CSIC, Glorieta de la Astronomía s/n, E-18008 Granada, Spain

⁴³Department of Astronomy, University of Maryland, College Park, 20742, USA

⁴⁴School of Earth and Space Exploration, Arizona State University, Tempe, AZ 85287-6004, USA

ABSTRACT

We report the identification of a pair of faint little red dots (LRDs), dubbed Red Eyes, in a strongly-lensed galaxy at $z \sim 7$ behind the PLCKG004.5-10.5 cluster, identified from the JWST Treasury program VENUS. Red Eyes are spatially resolved on the image plane with distinct colors, while the critical curve lies far north of Red Eyes, clearly requiring two different LRDs rather than a single LRD. Red Eyes is an extremely close pair of LRDs separated by ~ 70 pc in the source plane with a magnification of $\mu \sim 20$, which consistently explains another counter-image detected to the north-west. Red Eyes is hosted in a typical star-forming galaxy with $M_{\text{UV,int}} \sim -19$, but its own UV emission is very faint ($M_{\text{UV,int}} \gtrsim -16$). Moreover, Red Eyes does not reside at the galaxy center but lies at an offset position of approximately one effective radius R_e away from the galaxy center. If observed without lensing, Red Eyes would appear as a typical star-forming galaxy at $z \sim 7$ with $M_{\text{UV}} \sim -19$, showing no apparent LRD signatures in either morphology or SED. These results suggest that multiple off-center LRDs, similar to Red Eyes, may be commonly hidden in a typical high- z star-forming galaxy. In this case, various plausible scenarios may emerge, one of which is that intermediate-mass black holes (IMBHs) with $M_{\text{BH}} \sim 10^{4-6} M_{\odot}$ may form in star clusters on a stellar disk and contribute to the growth of the central supermassive black hole via mergers, with some IMBHs detectable as luminous LRDs in a sufficiently active and massive phase.

1. INTRODUCTION

James Webb Space Telescope (JWST) has identified a population of broad-line active galactic nuclei (AGNs) that exhibit a characteristic V-shaped spectral energy distribution (SED), with a blue UV continuum and a red optical continuum (e.g., D. D. Kocevski et al. 2023; Y. Harikane et al. 2023; J. Matthee et al. 2024; D. D. Kocevski et al. 2025; I. Labbe et al. 2025; V. Kokorev et al. 2024; H. B. Akins et al. 2025; J. E. Greene et al. 2024; C. C. Williams et al. 2024; T. S. Tanaka et al. 2025; K. Inayoshi & L. C. Ho 2025). These objects, commonly referred to as little red dots (LRDs), show extremely weak X-ray, mid-infrared, and radio emission, which challenges conventional AGN interpretations (M. Yue et al. 2024; H. B. Akins et al. 2025; T. T. Ananna et al. 2024; A. J. Gloudemans et al. 2025; R. Maiolino et al. 2025). While many LRDs exhibit only weak variability (C. J. Burke et al. 2025; M. Kokubo & Y. Harikane

2025; Z. Stone et al. 2025; W. L. Tee et al. 2025; Z. Zhang et al. 2025a), a multiply lensed LRD with a long time delay has been reported to show significant variability (Z. Zhang et al. 2025b). First identified at $z \gtrsim 4$, LRDs have recently also been found in the local universe, although with a significantly lower number density (Y. I. Izotov & T. X. Thuan 2008; X. Lin et al. 2025; R. Lin et al. 2025; X. Chen et al. 2025).

The several examples of strong Balmer breaks and Balmer absorption in the LRD spectra (e.g., R. P. Naidu et al. 2025; A. de Graaff et al. 2025a; X. Ji et al. 2025; K. Ronayne et al. 2025) have motivated the hypothesis that extremely dense neutral gas surrounding these candidate AGNs can produce such strong Balmer absorption features (e.g., K. Inayoshi & R. Maiolino 2025; D. Kido et al. 2025; K. Inayoshi et al. 2025). Theoretical studies suggest that these systems may represent an early accretion phase of AGNs (K. Inayoshi 2025), making

them a potentially crucial population for understanding the growth of supermassive black holes (SMBHs) and their coevolution with host galaxies.

These theoretical hypotheses assume that the red optical continuum arises from blackbody emission produced by the dense gas envelope surrounding the AGN, whereas the blue UV continuum originates from young stars in the associated galaxy. Although several studies have performed morphological decompositions of LRDs and their associated galaxy (M. Killi et al. 2024; Y. Zhang et al. 2025; P. Rinaldi et al. 2025; R. M. Mérida et al. 2025), isolating the galaxy components and deriving their physical properties remain challenging because of the extremely compact nature of LRDs. Several studies have also identified LRDs with blue companions with a few hundred pc to kpc scale offsets (R. M. Mérida et al. 2025; M. Golubchik et al. 2025; J. F. W. Baggen et al. 2025; C.-H. Chen et al. 2025a,b), which might be related to the UV emission from the LRDs. Gravitationally lensed LRDs are powerful probe for investigating the faint emission from the LRDs (L. J. Furtak et al. 2023a, 2024; R. M. Mérida et al. 2025; M. Golubchik et al. 2025; J. F. W. Baggen et al. 2025). However, the coevolution of the LRDs and the associated galaxy, or their connection to the SMBH growth, are still unclear.

In this work, we report the discovery of a pair of strongly lensed LRDs, dubbed Red Eyes, and an associated galaxy identified at $z \sim 7$ in PLCK G004-10.5 cluster by JWST/NIRCam observations. In Section 2, we present our observations and data reduction. In Section 3, we describe our analysis methods. Section 4 presents the results and their implications. We present our conclusions in Section 5. Throughout this paper, we assume cosmology parameters based on the TT, TE, EE + lowE + lensing + BAO result from Planck Collaboration et al. (2020) with $H_0 = 67.66 \text{ km s}^{-1} \text{ Mpc}^{-1}$, $\Omega_m = 0.30966$, and $\Omega_b = 0.04897$. All magnitudes are in the AB system (J. B. Oke & J. E. Gunn 1983).

2. OBSERVATIONS AND DATA REDUCTION

The galaxy cluster PLCK G004.5-10.5 ($z = 0.54$; C. Sifón et al. 2014; J. G. Albert et al. 2017; P. Tarrío et al. 2019; B. Salmon et al. 2020) was observed with JWST/NIRCam as part of the treasury lensing cluster survey Vast Exploration for Nascent, Unexplored Sources (VENUS; Cycle 4 GO-6882; PIs: S. Fujimoto & D. Coe; Fujimoto et al. in prep.) on 2025 October 4. The NIRCam observations utilize ten filters of F090W, F115W, F150W, F200W, F210M, F277W, F300M, F356W, F410M, and F444W with exposure times of 0.35–0.57 hours to homogeneously achieve a source detection limit of ~ 28 mag across all NIRCam

filters (5σ , point source). We also make use of archival HST ACS data taken in the RELICS survey (GO-10496; PI: D. Coe; D. Coe et al. 2019). PLCK G004.5-10.5 was observed on 2016 August 15th with F814W and on 2016 September 25th with F606W, with exposure times of 2377s and 2180s, achieving source detection limits of 27.1 and 27.6 mag, respectively.

Here, we briefly explain our data reduction procedure. We begin with JWST level-2 products from MAST and reduce them with the `grizli` pipeline (G. Brammer 2023a,b), which is similar to the method used for the widely available public DJA products. The photometric calibration was carried out with the Calibration Reference Data System (CRDS) context file `rwst_1456.pmap`. The `grizli` procedure incorporates crucial improvements over the standard STScI pipeline, including corrections for cosmic rays, stray light and detector artifacts (L. D. Bradley et al. 2023; J. Rigby et al. 2023). We further incorporate additional background, $1/f$ noise and diffraction spike subtraction, both at the amplifier level, for each filter, and then to the final drizzled mosaic (see, e.g., R. Endsley et al. 2024; V. Kokorev et al. 2025). JWST NIRCam images are then drizzled to a $0''.03$ /pix grid. The HST images are based on Gaia-aligned mosaics from the CHARGE archive (V. Kokorev et al. 2022), which are drizzled on the same footprint and pixel scale as the JWST data. A reduced color composite image is shown in Figure 1. More details of the data reduction will be presented in a separate paper.

3. ANALYSIS

3.1. Photometry and LRD Selection

We produce a detection image by taking an inverse variance-weighted mean of the point spread function (PSF)-matched images of F200W, F277W, F356W, and F444W. Source detection is conducted on the detection image using `Photutils` (L. Bradley et al. 2025). We then measure isophotal fluxes to obtain reliable SEDs for objects with complex morphology due to the strong gravitational lensing. We measure the total flux of each filter with an isophotal aperture, which is determined by a region 5σ above the background with the detection image.

Using the photometry measured above, we select objects that meet the LRD selection criteria presented in I. Labbe et al. (2025):

$$F150W - F200W < 0.8 \quad (1)$$

$$F277W - F356W > 0.7 \quad (2)$$

$$F277W - F444W > 1.0, \quad (3)$$

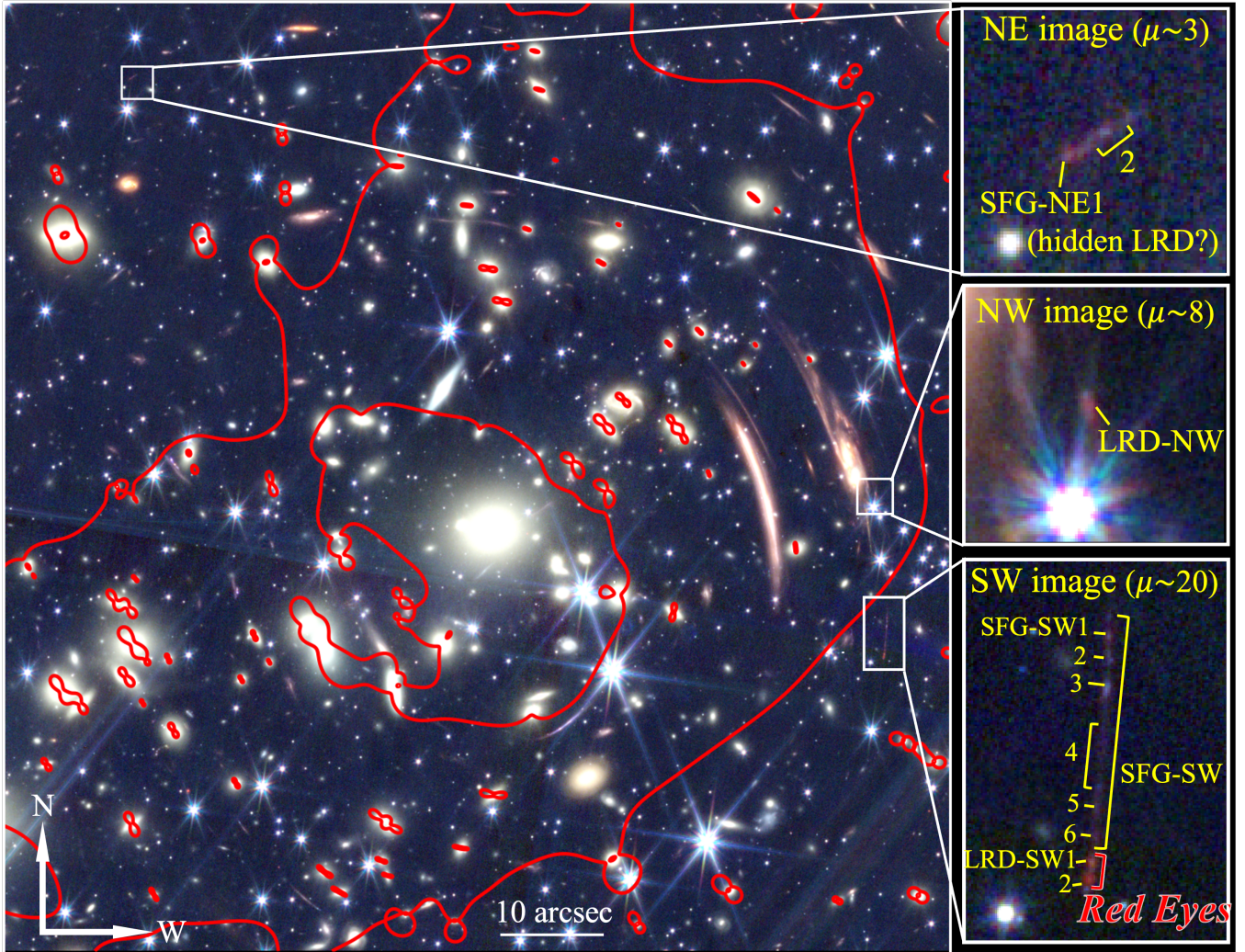


Figure 1. RGB composite image (R: F356W+F444W, G: F200W+F277W, B: F115W+F150W) of the PLCK G004-10.5 cluster. The red contours indicate the critical curves at $z = 7.4$. LRD and SFG images are highlighted by annotated inset figures.

which selects objects with blue UV and red optical continuum at $z = 6 - 9$ (the top panels of Figure 2). We do not include the compactness criterion to avoid excluding LRDs with complex morphologies, such as those with extended host galaxies or closely separated multiple LRDs. Among the objects satisfying the above criteria, we identify LRD-SW1 and LRD-SW2, which are located near the end of an arc extending $\sim 5''$ (Figure 1). Hereafter, we refer to LRD-SW1 and 2 as “Red Eyes.” While Red Eyes show clear V-shaped SEDs, which is a typical feature of LRDs, the rest of the arc does not show red optical continua (Figure 3) but instead shows an SED typical of star-forming galaxies (SFGs). Red Eyes and the arc all present clear non-detection blueward of F115W and strong excess in F410M, indicating that they are located at the same redshift, and that the arc is an SFG associated with Red Eyes. We thus refer to the

arc as SFG-SW. SFG-SW consists of six diffuse components, aligned from north to south and labeled SFG-SW1 through SFG-SW6. Based on a gravitational lens model (Section 3.3), we also identify a counter-images in north-west and north-east region (Figure 1; hereafter NW and NE images, respectively), which have similar colors to Red Eyes. Because the NW image appears to be contaminated by the light from a nearby bright star, we fit the PSF of each band to the star and subtract it before performing photometry. We then identify LRD-NW, which also satisfies the color selection criteria (Figure 2), although the detection of a galaxy near the NW image remains marginal due to the nearby bright star. There are two distinct extended sources in the NE image, which do not satisfy the color selection criteria (Figure 2). They are hereafter referred to as SFG-NE1 and 2, although SFG-NE1 shows a mildly V-shaped SED. A

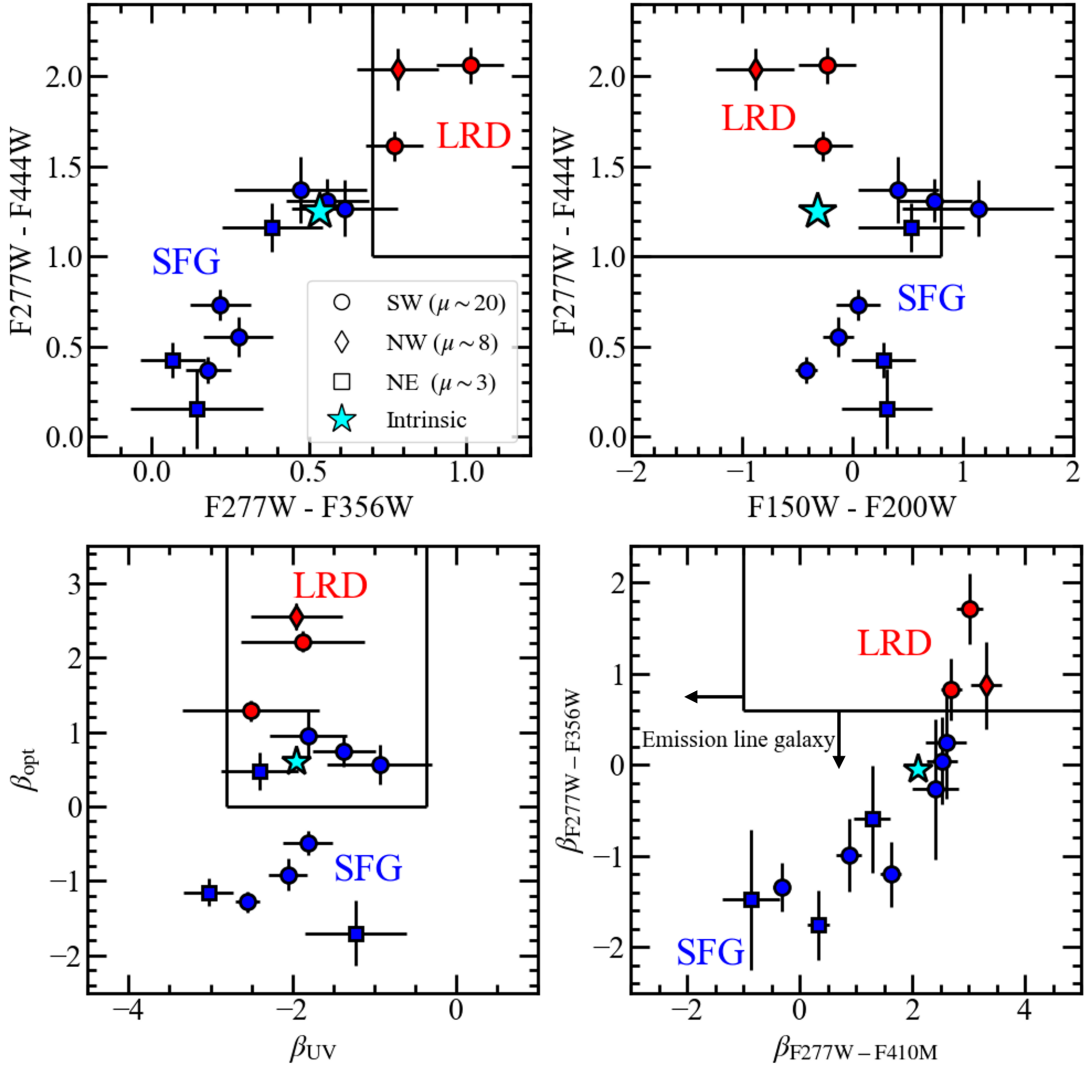


Figure 2. LRD selection using colors (the top panels) and slope fitting (the bottom panels). The black lines show the LRD selection threshold. The red and blue symbols indicate the LRD and SFG images, respectively. The circles, diamonds, and squares represent the SW, NW, and NE images, respectively. The LRD-SW1, SW2, and NW satisfy all of the LRD selection criteria, while the SFG components do not. The cyan stars denote the intrinsic colors and slopes of the whole system (i.e., corrected for the gravitational lensing; Section 4.2). Without gravitational lensing, Red Eyes would not be identified as an LRD.

possible explanation for the less red optical continuum of SFG-NE1 is presented in Section 4.2.

We also perform power-law fitting to the UV and optical slopes to see whether these objects satisfy the selection criteria presented in *D. D. Kocevski et al. (2025)*:

$$-2.8 < \beta_{UV} < -0.37 \quad (4)$$

$$\beta_{opt} > 0, \quad (5)$$

where β_{UV} and β_{opt} are the UV and optical slopes, respectively. β_{UV} is measured with F115W, F150W, and F200W, whereas β_{opt} is measured with F277W, F356W, and F444W. The bottom left panel of Figure 2 shows β_{UV} and β_{opt} values for the LRD and SFG images. We

find that all LRD images satisfy the slope selection criteria within the error. *D. D. Kocevski et al. (2025)* introduced additional selection criteria for objects with $z < 8$ to exclude emission line galaxies using $\beta_{F277W-F356W}$, and $\beta_{F277W-F410M}$, which are the power-law slopes measured with the two bands described in the subscripts. We use

$$\beta_{F277W-F356W} > 0.6 \quad (6)$$

$$\beta_{F277W-F410M} > -1, \quad (7)$$

where the lower limit on $\beta_{F277W-F356W}$ is equivalent to the color cut $F277W - F356W > 0.7$. The bottom right panel of Figure 2 shows $\beta_{F277W-F356W}$ and

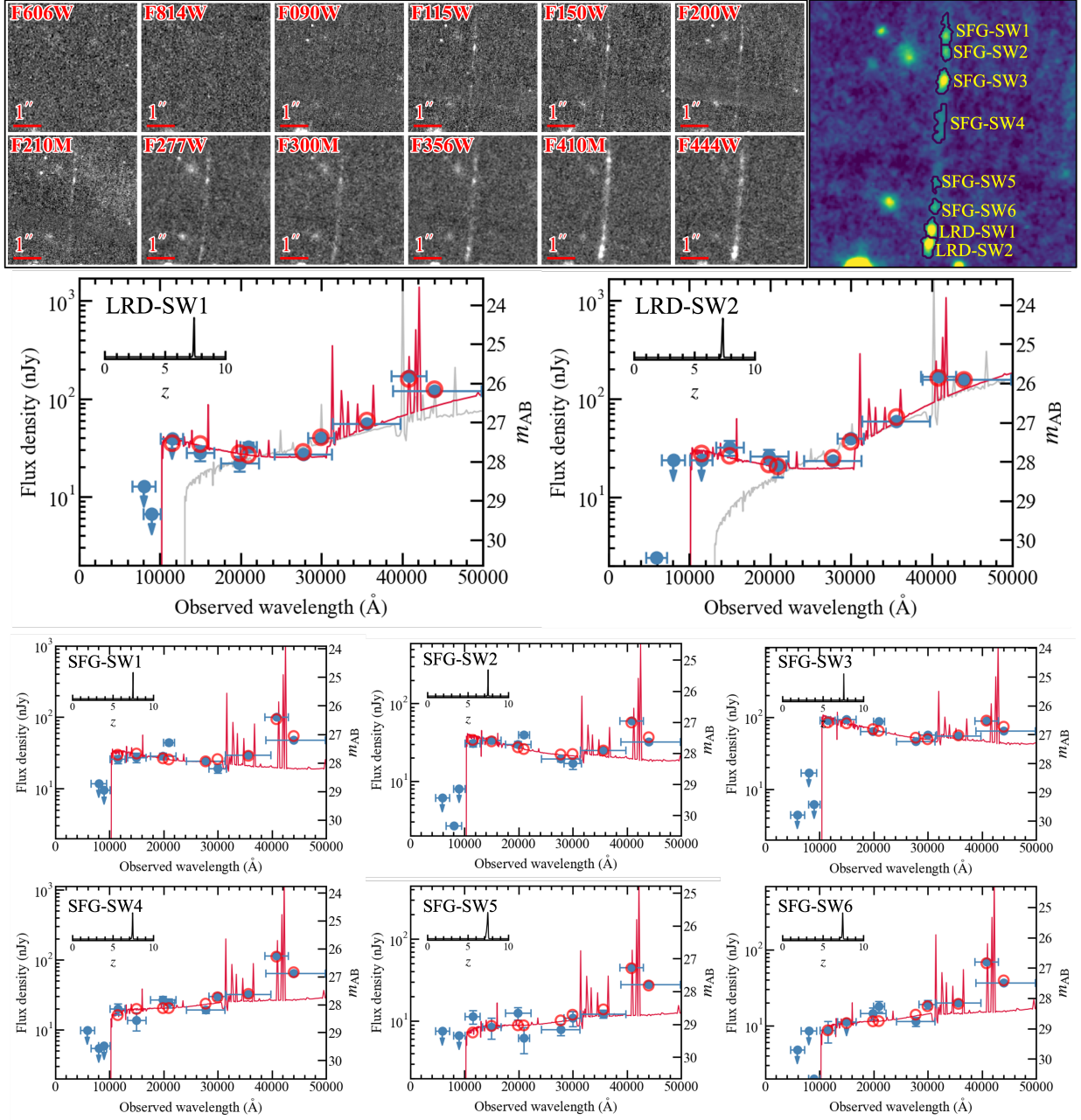


Figure 3. (Top) HST and NIRCам cutouts of the SW image. The rightmost panel represents the segmentation image. (Bottom) Photometry and best-fit SEDs for the SW images. The blue points indicate the observed photometry, with upper limits shown at the 3σ level. The photometry and upper limit values are not corrected for the magnification. The red curves show the best-fit SEDs consisting of galaxy and blackbody components, while the red circles indicate the best-fit photometry. The gray curves in the bottom two panels represent the best-fit SEDs without the blackbody component. The models without the blackbody component favor the solutions invoking dusty SFGs, which significantly underestimate the UV continuum due to the strong dust attenuation. The posterior redshift distribution is shown in the top-left corner of each panel.

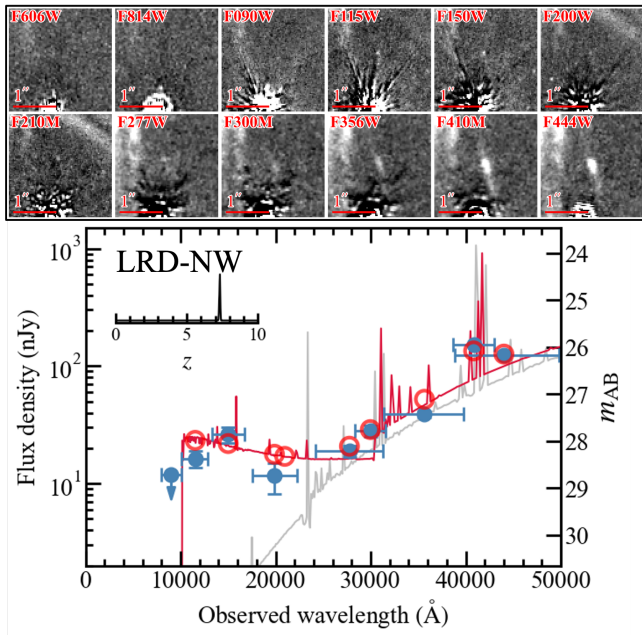


Figure 4. Same as Figure 3, but for the NW image.

$\beta_{F277W-F410M}$. We find that all LRD images satisfy these criteria, indicating that the red optical slopes are not solely the result of strong emission lines. Several SFG components satisfy a subset of the selection criteria, but not all of them. Although these components exhibit slightly red optical colors, their SEDs can be explained by emission-line galaxies (Section 4.1).

3.2. SED Fitting

We conduct SED fitting to the LRD and SFG images using BAGPIPES (A. C. Carnall et al. 2018). For stellar emission, we assume a BPASS stellar population synthesis model (E. R. Stanway & J. J. Eldridge 2018) with delayed- τ star-formation histories (SFHs). We adopt flat priors on stellar age $t_{\text{age}} \in [0.01, 5]$ Gyr, star-formation timescale $\tau \in [0.1, 3]$ Gyr, stellar metallicity $Z_* \in [0.1, 1] Z_{\odot}$, and log of stellar mass $\log_{10}(M_*/M_{\odot}) \in [5, 13]$. For nebular emission, we run version 23 of the Cloudy photoionization code (G. J. Ferland et al. 1998; C. M. Gunasekera et al. 2023) using the BPASS spectra as incident radiation and obtain grids of nebular emission. We adopt a flat prior on the ionization parameter $\log_{10} U \in [-4, -1]$, and the nebular metallicity is assumed to be the same as the stellar metallicity. For dust extinction, we assume a D. Calzetti et al. (1994) extinction law with a flat prior on the total extinction $A_V \in [0, 5]$ mag. The redshift prior is set to $z \in [0, 10]$. In addition to the galaxy model fitting explained above, to model the red optical continuum observed in the LRDs, we follow the method described in

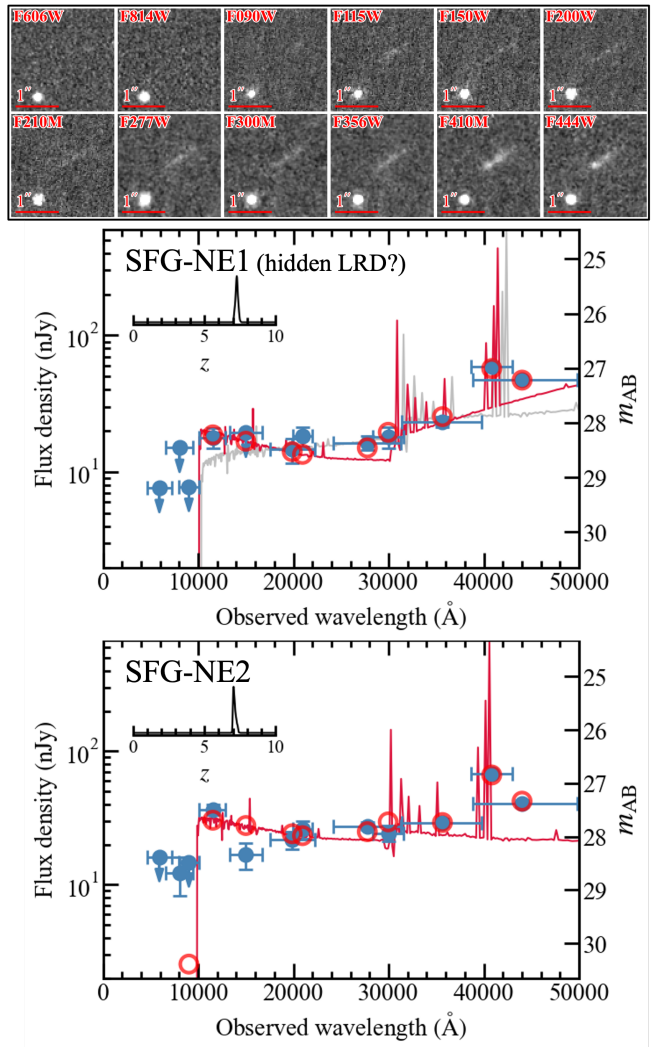


Figure 5. Same as Figure 3, but for the NE image.

A. de Graaff et al. (2025b) and H. Umeda et al. (2025) and include a blackbody function:

$$f_{\nu} \propto B_{\nu}(T_{\text{BB}})H(x), \quad (8)$$

where $B_{\nu}(T_{\text{BB}})$ is the Planck function of temperature T_{BB} . We take into account the Balmer break by introducing the Heaviside step function $H(x)$, where $x = \nu - c/\lambda_{\text{Balmer}}$ and $\lambda_{\text{Balmer}} = 3646 \text{ \AA}$. We adopt flat priors on T_{BB} , allowing $T_{\text{BB}} \in [4000, 6000]$ K following H. Umeda et al. (2025). In the blackbody fitting, we fix $A_V = 0$, motivated by the negligible dust content in the LRDs and by the need to avoid degeneracy with T_{BB} . We also impose a constraint on the blackbody fit such that the Balmer break wavelength is shorter than F356W, in order to prevent an unphysically strong Balmer break from mimicking the red optical continuum. We perform SED fitting with and without blackbody emission to all components.

3.3. Gravitational Lens Modeling

A gravitational lens model for the PLCKG004.5-10.5 cluster is constructed based on a revised version of the parametric method by A. Zitrin et al. 2015 (for more details, see also M. Pascale et al. 2022; L. J. Furtak et al. 2023b). In this model, cluster member galaxies are described by double Pseudo-Isothermal Ellipsoids (dPIE; Á. Elíasdóttir et al. 2007), and the large-scale dark matter distribution is represented by a diffuse halo modeled as a Pseudo-Isothermal Elliptical Mass Distribution (PIEMD; e.g. C. R. Keeton 2001). We use 10 multiple image systems as constraints, 8 confirmed with spectroscopy for at least one image. Cluster members are selected by matching the red sequences formed in the NIRCam/F090W and F150W; ACS/F814W and NIRCam/F150W; and ACS/F606W and F814W spaces, together with data from MUSE. For minimization, we adopt a positional uncertainty of $0''.1$ for all images. All multiple images are reproduced by the model with a Δ RMS between model and observations of $0''.57$. Adopting the best-fit model yields magnification factors for the SW, NW, and NE images at $z \sim 7.4$ of $\mu \sim 20$, 8, and 3, respectively.

4. RESULTS AND DISCUSSION

4.1. SEDs of Individual Component

Figures 3, 4, and 5, show the SED-fitting results for each component. The photometric redshifts of the individual components are generally consistent at $z \sim 7.4$. The BAGPIPES fits that include a blackbody component reproduce both the blue UV continuum and the red optical continuum observed in the LRD images. Without this component, the best-fit solutions require dusty star-forming galaxy templates to match the red optical continuum, which in turn leads to a significant underestimate of the UV flux. In contrast, the SFG components are well-explained by young star-forming galaxy models. We note that the fits to the SFG images with and without the blackbody component yield nearly identical best-fit SEDs, implying little contribution from the blackbody component. For the LRD images, the best-fit T_{BB} values are ~ 4000 – 4500 K, which are slightly lower than theoretical predictions of ~ 5000 K from the black hole envelope models (D. Kido et al. 2025; K. Inayoshi et al. 2025) but consistent with the JWST/PRISM spectroscopy demographic study of A. de Graaff et al. (2025b).

4.2. Source Plane Reconstruction

Using the gravitational lens model established in Section 3.3, we reconstruct a source plane image. We uti-

lize `Lenstruction`¹ (L. Yang et al. 2020), which is built based on `Lenstronomy`² (S. Birrer & A. Amara 2018; S. Birrer et al. 2021). `Lenstruction` performs forward modeling to reconstruct the source brightness distribution, considering the broadening due to the PSF.

As shown in Figure 1, the critical curve does not cross between the LRD-SW1 and 2. This indicates that the two LRD images are not multiple images of a single LRD, but instead represent two distinct LRDs on the source plane. While they are not fully resolved in the NE and NW images owing to their relatively low magnifications, they are clearly deblended in the SW image³.

We thus use two Gaussian profiles, whose widths σ are fixed at 10^{-3} arcsec, well below the FWHMs of the NIRCam PSFs, to describe the two LRD images. To reproduce the SFG components, we model the diffuse emission covering the entire arc with a single elliptical Sérsic profile and the clumpy emission (SFG-SW1, 2, 3, and 6) with three Gaussian profiles, allowing the widths of the Gaussian profiles to vary freely. To avoid a degeneracy, the Sérsic index n is fixed at 1. The fitting is conducted to the F444W image of the SW image, which have the high S/N ratio (multi-band fitting is conducted later in this section). The result is presented in Figure 6. The two Gaussian profiles successfully explain LRD-SW1 and 2. The intrinsic two LRDs corresponding to LRD-SW1 and LRD-SW2 are hereafter referred to as LRD1 and LRD2, respectively. The other Gaussian and Sérsic profiles reproduce the clumpy morphology within the diffuse arc. The three clumps explained by the Gaussian are referred to as star-forming (SF) clumps 1 to 3 from north to south. The source plane image is shown in the rightmost panel of Figure 6. LRD1 and LRD2 are separated by a distance of ~ 70 pc (physical), which is much smaller than those of known dual LRDs (a few kpc; T. S. Tanaka et al. 2024; R. M. Mérida et al. 2025). The two LRDs are located at a distance of ~ 460 pc from the center of the SFG, which is similar to several offsets reported in previous LRD studies, such as blue com-

¹ <https://github.com/yilian/lenstruction>

² <https://github.com/lenstronomy/lenstronomy>

³ If we consider a small perturber in between LRD-SW1 and 2, this could split a single LRD image into multiple images. At this position relative to the critical curve, such a perturber would produce three counter-images very close to each other, not two. For a sufficiently small perturber, two of the images could merge into a single one, leaving only two visible images as seen in the JWST data. However, in such a scenario, the flux of one of the counter-images (the unresolved pair) would be significantly higher than the other, which is inconsistent with the observations. Furthermore, there is no evidence of the perturber in the images, making this explanation highly unlikely.

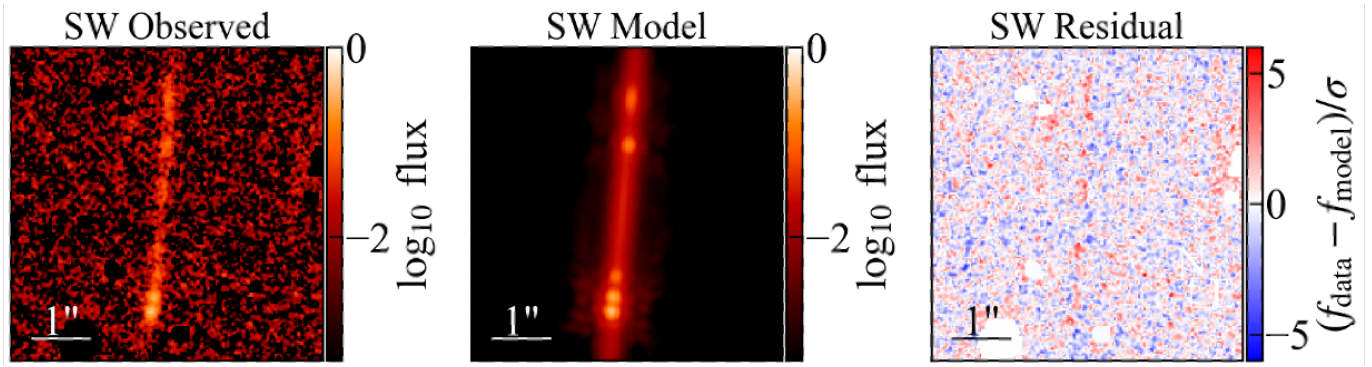


Figure 6. Source plane reconstruction. From left to right, each column represents the observed, modeled, residual of the F444W image.

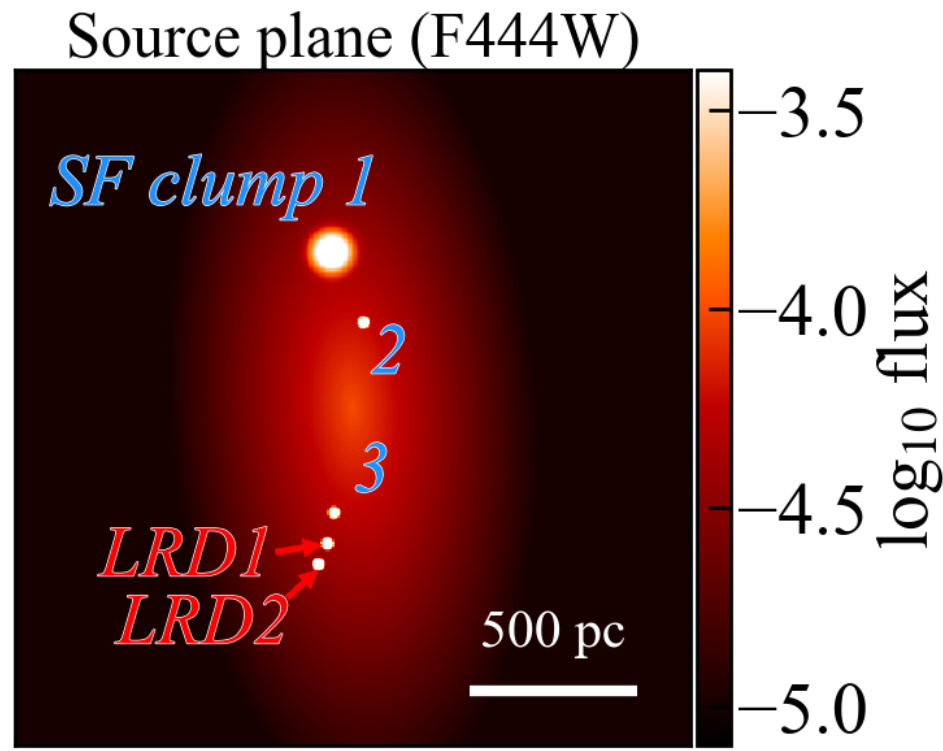


Figure 7. Source plane image. The scale bar indicates 500 physical pc at $z = 7.4$.

panions observed near LRDs (e.g., M. Golubchik et al. 2025; J. F. W. Baggen et al. 2025) and off-centered diffuse emission around LRDs (C.-H. Chen et al. 2025a; P. Rinaldi et al. 2025). The half light radius of the SFG is ~ 410 pc, which corresponds to the typical size of star-forming galaxies at this redshift and luminosity (e.g., T. Shibuya et al. 2019; Y. Ono et al. 2025; T. Morishita et al. 2024; T. B. Miller et al. 2025).

Next, we conduct multi-band fitting to investigate the intrinsic SEDs of the LRDs and SFG. We fit the amplitudes of the elliptical Sérsic and Gaussian profiles to each band, while keeping all other parameters fixed to the best-fit values obtained with F444W. We then integrate

the surface brightness distributions of the Sérsic and Gaussian profiles to obtain the total flux of each component. Figure 8 presents the intrinsic SEDs of the two LRDs and SFG (sum of the Sérsic profile and three SF clumps). Interestingly, the intrinsic luminosity of the LRDs ($M_{UV,int} \gtrsim -16$) are ~ 20 times fainter than that of the SFG ($M_{UV,int} \sim -19$), indicating that these LRDs will totally be lost in the light of the SFG without gravitational lensing. In Figure 2, the colors and slopes of the intrinsic SED of the whole system are presented in cyan, indicating that this system would not be identified as an LRD in the absence of gravitational lensing. This effect is already seen in SFG-NE1, which moderately ex-

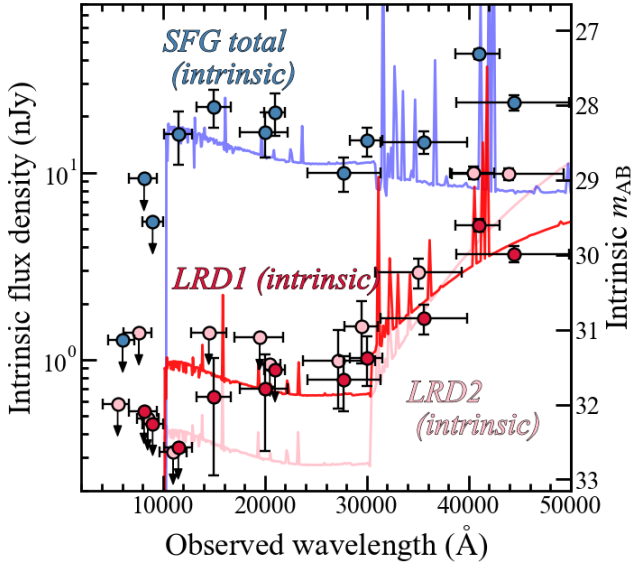


Figure 8. Intrinsic SEDs obtained by multi-band source plane reconstruction (Section 4.2). The blue points indicate the SED for the SFG (sum of all of the star-forming clumps and diffuse component), while the red and pink points represent that for each of the LRD pair.

hibits the V-shaped SED but does not satisfy the LRD selection criteria due to the relatively low magnification. We note that the rest-UV emission from the LRDs is detected in Figure 3, but not in Figure 8, as the extended wings of the Sérsic profile dominate the UV light in the vicinity of the LRDs. This is consistent with a scenario in which the V-shaped SEDs observed in LRDs arise from a combination of blue UV emission from their host galaxies and red optical emission associated with black holes.

We conduct the BAGPIPES fitting to the intrinsic SEDs in the same manner as described in Section 3.2. Figure 8 presents the best-fit SED, showing a solution of a young SFG. The intrinsic SFG has a stellar mass of $\log(M_*/M_\odot) = 8.0^{+0.1}_{-0.1}$, stellar age of 90^{+40}_{-20} Myr and SFR of $1.3^{+0.3}_{-0.3} M_\odot/\text{yr}$. The left panel of Figure 9 shows the relation between SFR and stellar mass. The SFG in this work is located on the star-forming main sequence (SFMS), indicating that it corresponds to the typical SFG at this redshift. The right panel of Figure 9 presents the size-mass relation, where we find that the host galaxy has a typical size at this redshift and stellar mass.

4.3. Mock Observation without Gravitational Lensing

Owing to strong gravitational lensing, we are able to observe a pair of faint LRDs associated with an intrinsically dominant, otherwise typical SFG. To investigate how such a system would appear without gravitational

lensing, we generate a mock image by convolving the source-plane image with the F444W PSF (Figure 10). For comparison, we present an example of a typical star-forming galaxy, CEERS-48628 (S. L. Finkelstein et al. 2022), which has a similar redshift ($z_{\text{spec}} = 7.2$) and UV luminosity ($M_{\text{UV}} = -19.5$). The mock image resembles typical SFGs at similar redshifts, and the LRDs are completely undetectable. This suggests that we may be missing such faint and multiple LRD systems associated with ordinary SFGs in the absence of strong gravitational lensing.

4.4. Implications for SMBH Formation

Here we discuss the implications for SMBH formation based on the multiple, off-center, faint LRDs. To estimate the black hole masses of LRD1 and LRD2, we follow the methodology presented in H. Umeda et al. (2025), assuming that the bolometric luminosity of an LRD (L_{bol}) equals to the luminosity of the blackbody emission. This assumption is motivated by the presence of hypothetical gaseous envelopes enshrouding the accreting black hole, whose thermal spectra explain the spectral features of LRDs (D. Kido et al. 2025; K. Inayoshi et al. 2025), and the bolometric correction is supported for some LRDs that have multi-wavelength observations including MIRI photometry (J. E. Greene et al. 2025; K. Ronayne et al. 2025). The L_{bol} values of LRD1 and LRD2 are shown in Figure 11. For comparison, we also present L_{bol} values of LRDs with similar host stellar masses ($M_* \sim 10^8 M_\odot$) reported in H. Umeda et al. (2025), which are not gravitationally lensed. LRD1 and LRD2 have $L_{\text{bol}} = 3.3^{+0.5}_{-0.4} \times 10^{42} \text{ erg s}^{-1}$ and $6.8^{+0.4}_{-0.4} \times 10^{42} \text{ erg s}^{-1}$, which is significantly lower than those of previously reported LRDs.

We estimate M_{BH} using the following equation:

$$M_{\text{BH}} = \frac{\sigma_{\text{T}}}{4\pi c G m_{\text{p}}} \cdot \frac{L_{\text{bol}}}{\lambda_{\text{Edd}}} \quad (9)$$

$$\simeq 0.81 \times 10^5 M_\odot \lambda_{\text{Edd}}^{-1} \left(\frac{L_{\text{bol}}}{10^{43} \text{ erg s}^{-1}} \right), \quad (10)$$

where σ_{T} , c , G , and m_{p} are the Thomson scattering cross section, the speed of light, the gravitational constant, and the proton mass, respectively. λ_{Edd} denotes the Eddington ratio. Following H. Umeda et al. (2025), we assume $\lambda_{\text{Edd}} = 0.1 - 1$ with a fiducial value of 0.5, which is motivated by the near-Eddington accretion phase expected in the BHE model. The inferred black hole masses of LRD1 and LRD2 are $\log M_{\text{BH}}/M_\odot = 4.4^{+0.7}_{-0.7}$ and $4.1^{+0.8}_{-0.4}$, respectively, placing them in the intermediate-mass black hole (IMBH) regime ($M_{\text{BH}} < 10^5 M_\odot$). If faint, off-center, multiple LRDs are commonly present in typical SFGs, several possibilities may

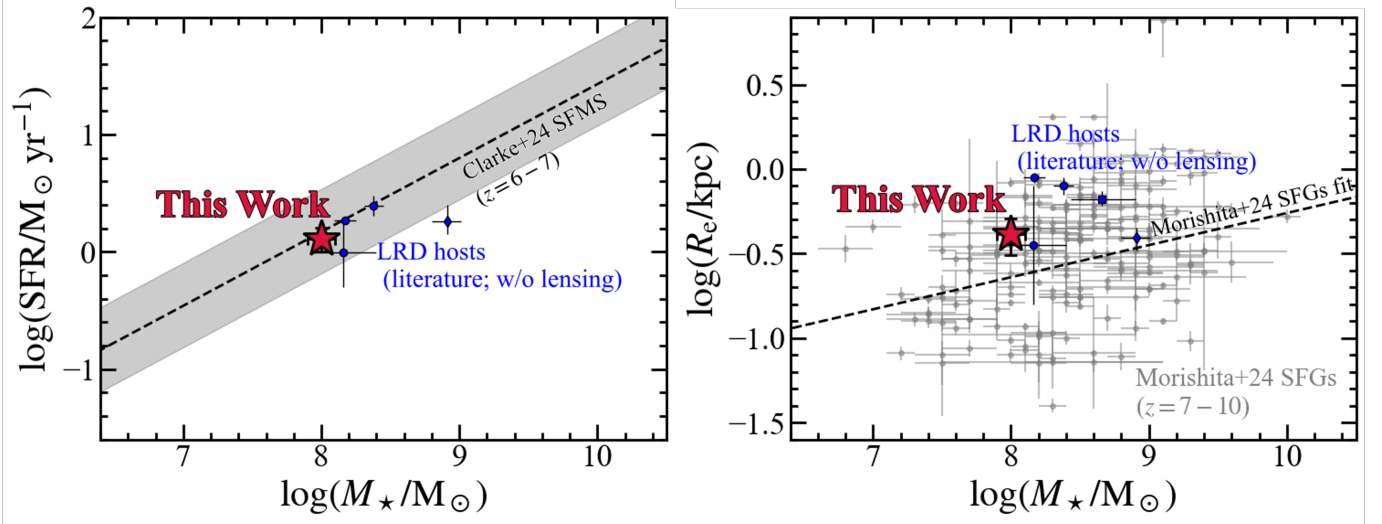


Figure 9. (Left) SFR-stellar mass relation. The red and blue symbols are the same as the left figure. The black dashed line and gray shaded region are the best-fit relation and its uncertainty for SFMS presented in L. Clarke et al. (2024). (Right) Size-mass relation. The red star shows the SFG in this work. The blue points represent the LRD hosts presented in literature (circle: C.-H. Chen et al. 2025a; square: C.-H. Chen et al. 2025b; diamond: Y. Zhang et al. 2025.) The gray points and black dashed line indicate SFG sample and linear regression to it presented in (T. Morishita et al. 2024).

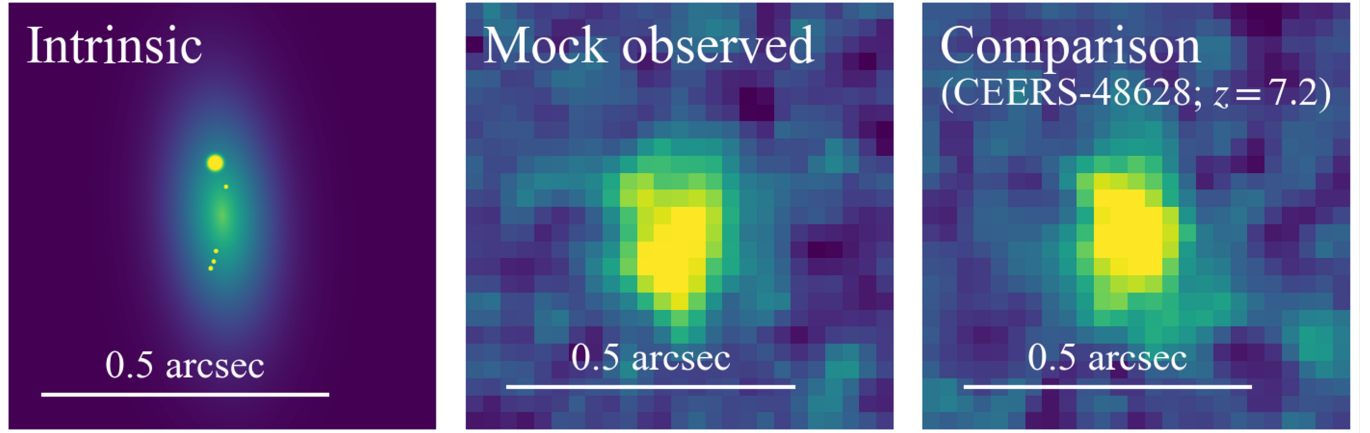


Figure 10. NIRCcam F444W mock image without gravitational lensing. (Left) Intrinsic image obtained from the source plane reconstruction (Section 4.2). (Middle) Mock observed image obtained by convolving the NIRCcam PSF to the intrinsic image. (Right) Example image of the typical SFG (CEERS-48628; S. L. Finkelstein et al. 2022), which has the similar redshift and luminosity as the SFG in this work.

be considered. one potential scenario is that multiple IMBHs form at off-nuclear locations, possibly within massive star clusters (e.g., S. F. Portegies Zwart & S. L. W. McMillan 2002; S. F. Portegies Zwart et al. 2004; Y. Sakurai et al. 2017; M. S. Fujii et al. 2024), and subsequently migrate toward the galaxy center by dynamical friction, eventually contributing to the growth of a central SMBH via mergers (e.g., A. Dekel et al. 2025). Following J. Binney & S. Tremaine (2008) and H. Übler et al. (2025), we estimate the dynamical friction timescale, t_{df} , for the two LRDs to migrate to the galaxy center using the following equation:

$$t_{\text{df}} = \frac{1.65}{\ln \Lambda} \frac{R^2 \sigma_*}{GM_{\text{BH}}}, \quad (11)$$

where R is the distance between the LRD and the galactic center (~ 460 pc), and σ_* is the stellar velocity dispersion. We assume $\sigma_* = 20$ km s $^{-1}$ based on the $M_* - \sigma_*$ relation from J. E. Greene et al. (2020) at $M_* \sim 10^8 M_\odot$. $\ln \Lambda$ is the Coulomb logarithm, with $\Lambda \approx M_*/M_{\text{BH}}$. We obtain $t_{\text{df}} = 0.15$ Gyr, which corresponds to a merger at $z \sim 6$. The off-center faint LRDs can thus migrate to the galactic center well within the available cosmic time, possibly contributing to SMBH

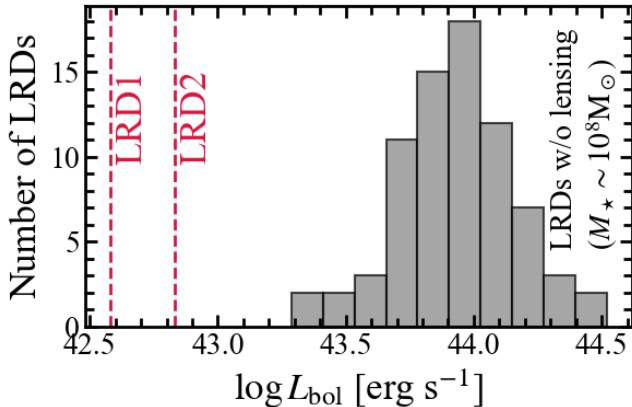


Figure 11. Bolometric luminosity distribution of LRDs. The red dashed lines indicate LRD1 and LRD2. The gray histogram shows the LRDs presented in *H. Umeda et al. (2025)*, who estimate L_{bol} of the LRD sample presented in *H. B. Akins et al. (2025)* based on the black hole envelope model (*D. Kido et al. 2025; K. Inayoshi et al. 2025*).

growth via mergers. A somewhat more exotic variant of such a dynamically-driven scenario could involve massive primordial black holes, naturally leading to multiple faint AGN in close proximity (e.g., *S. Zhang et al. 2025*).

Alternatively, the low L_{bol} values may be attributed to low λ_{Edd} , rather than intrinsically low black hole masses, implying an inactive or weakly accreting phase. *K. Inayoshi et al. (2025)* argue that the LRD is sustained by near-Eddington accretion onto a neutral gas envelope surrounding the black hole, and that the LRD phase terminates once the accretion rate drops well below the Eddington limit. In this context, Red Eyes may represent a system observed at the very end of the LRD phase, providing a unique opportunity to investigate the evolutionary connection between LRDs and normal AGNs or QSOs.

5. SUMMARY

In this work, we present the detection of a very close pair of LRDs found in a strongly lensed galaxy and separated by ~ 70 pc, which are embedded in the typical SFGs at $z \sim 7$. The main findings in this work are summarized below:

- We identify a strongly lensed arc ($\mu \sim 20$) at $z \sim 7$ that contains two point-like objects satisfying the LRD color selection criteria. The critical curve at $z \sim 7$ does not pass between the two LRD images, indicating that they are not multiple images of a single source, but instead correspond to two distinct objects on the source plane. In contrast, the extended arc exhibits a blue SED, implying that it

is a star-forming galaxy associated with the LRDs. Source-plane reconstruction reveals that the two LRDs are separated by only ~ 70 pc and are offset from the galaxy center by ~ 460 pc, comparable to the galaxy’s effective radius.

- The intrinsic SEDs of the two LRDs are much fainter than that of the associated galaxy, indicating that the flux from the LRDs would be completely overwhelmed by that of the host galaxy in the absence of gravitational lensing. Mock NIR-Cam observations further show that such a system would resemble typical star-forming galaxies at similar redshifts without gravitational lensing. These analyses suggest that, without magnification, many of these LRDs may be unnoticed inside normal SFGs.

ACKNOWLEDGMENTS

This work is based on observations made with the NASA/ESA/CSA James Webb Space Telescope. The data were obtained from the Mikulski Archive for Space Telescopes (MAST) at the Space Telescope Science Institute (STScI), which is operated by the Association of Universities for Research in Astronomy (AURA), Inc., under NASA contract NAS 5-03127 for JWST. The JWST observations are associated with program #6882 (VENUS) and #1345. This paper is also based on observations made with the NASA/ESA Hubble Space Telescope. The data were obtained from MAST at STScI, which is operated by AURA under NASA contract NAS 5-26555. The HST observations are associated with program #14096 (RELICS). The authors acknowledge the use of the Canadian Advanced Network For Astronomy Research (CANFAR) Science Platform operated by the Canadian Astronomy Data Center (CADC) and the Digital Research Alliance of Canada (DRAC) with support from the National Research Council for Canada (NRC), the Canadian Space Agency (CSA), CANARIE, and the Canadian Foundation for Innovation (CFI).

HY acknowledges support by KAKENHI (25KJ0832) through Japan Society for the Promotion of Science (JSPS). SF acknowledges support from the Dunlap Institute, funded through an endowment established by the David Dunlap family and the University of Toronto. MO acknowledges the supports from the World Premier International Research Center Initiative (WPI Initiative), MEXT, Japan, the joint research program of the Institute for Cosmic Ray Research (ICRR), the University of Tokyo, and KAKENHI (20H00180, 21H04467, 25H00674) through Japan Society for the Promotion

of Science (JSPS). VK acknowledge support from the University of Texas at Austin Cosmic Frontier Center. MO is supported by JSPS KAKENHI Grant Numbers JP25H00662, JP22K21349. AZ acknowledges support by the Israel Science Foundation Grant No. 864/23. MN acknowledges support from KAKENHI Grant Nos. 25KJ0828 through Japan Society for the Promotion of Science (JSPS). UH acknowledges support through grants KAKENHI (23KJ0646) through Japan Society for the Promotion of Science (JSPS). HA acknowledges support from CNES, focused on the JWST mission, and the French National Research Agency (ANR) under grant ANR-21-CE31-0838. FEB acknowledges support from ANID-Chile BASAL CATA FB210003, FONDECYT Regular 1241005, and ECOS-ANID ECOS240037. JMD acknowledges the support of projects PID2022-138896NB-C51 (MCIU/AEI/MINECO/FEDER, UE) Ministerio de Ciencia, Investigación y Universidades and SA101P24. YH acknowledges support from the Japan Society for the Promotion of Science (JSPS) Grant-in-Aid for Scientific Research (24H00245) and the JSPS International Leading Research (22K21349). KI acknowledges support from the National Natural Science Foundation of China (12573015, 1251101148, 12233001), the Beijing Natural Science Foundation (IS25003), and the China Manned Space Program (CMS-CSST-2025-A09). RPN is grateful for the generous support of Neil and Jane Pappalardo through the MIT Pappalardo Fellowship. PD warmly acknowledges support from an NSERC discovery grant (RGPIN-2025-06182). RA acknowledges support of Grant PID2023-147386NB-I00 funded by MICIU/AEI/10.13039/501100011033 and by ERDF/EU. GEM acknowledges the Villum Fonden research grants 37440 and 13160. MB acknowledges sup-

port from the ERC Grant FIRSTLIGHT and Slovenian national research agency ARIS through grants N1-0238 and P1-0188. The Cosmic Dawn Center (DAWN) is funded by the Danish National Research Foundation under grant DNRFF140. EV acknowledges financial support through grants INAF GO Grant 2024 “Mapping Star Cluster Feedback in a Galaxy 450 Myr after the Big Bang” and the European Union – NextGenerationEU within PRIN 2022 project n.20229YBSAN - Globular clusters in cosmological simulations and lensed fields: from their birth to the present epoch. MGO acknowledges financial support from the State Agency for Research of the Spanish MCIU through Center of Excellence Severo Ochoa award to the Instituto de Astrofísica de Andalucía CEX2021-001131-S funded by MCIN/AEI/10.13039/501100011033, and from the grant PID2022-136598NB-C32 “Estallidos8”. MGO also acknowledges the support by the project ref. AST22_00001.Subp_11 funded from the EU – NextGenerationEU, PPCC Junta de Andalucía. PAAL thanks the support from CNPq, grants 310260/2025-6 and 404160/2025-5, and FAPERJ, grant E-26/200.545/2023. RAW acknowledges support from NASA JWST Interdisciplinary Scientist grants NAG5-12460, NNX14AN10G and 80NSSC18K0200 from GSFC.

Facilities: HST, JWST

Software: BAGPIPES (A. C. Carnall et al. 2018), BPASS (E. R. Stanway & J. J. Eldridge 2018), Cloudy (C. M. Gunasekera et al. 2023), grizli (G. Brammer 2023a,b), Lenstronomy (S. Birrer & A. Amara 2018; S. Birrer et al. 2021), Lenstruction (L. Yang et al. 2020) Photutils (L. Bradley et al. 2025)

REFERENCES

- Akins, H. B., Casey, C. M., Lambrides, E., et al. 2025, ApJ, 991, 37, doi: [10.3847/1538-4357/ade984](https://doi.org/10.3847/1538-4357/ade984)
- Albert, J. G., Sifón, C., Stroe, A., et al. 2017, A&A, 607, A4, doi: [10.1051/0004-6361/201730496](https://doi.org/10.1051/0004-6361/201730496)
- Ananna, T. T., Bogdán, Á., Kovács, O. E., Natarajan, P., & Hickox, R. C. 2024, ApJL, 969, L18, doi: [10.3847/2041-8213/ad5669](https://doi.org/10.3847/2041-8213/ad5669)
- Baggen, J. F. W., van Dokkum, P., Labbé, I., & Brammer, G. 2025, arXiv e-prints, arXiv:2512.03239, doi: [10.48550/arXiv.2512.03239](https://doi.org/10.48550/arXiv.2512.03239)
- Binney, J., & Tremaine, S. 2008, Galactic Dynamics: Second Edition
- Birrer, S., & Amara, A. 2018, Physics of the Dark Universe, 22, 189, doi: [10.1016/j.dark.2018.11.002](https://doi.org/10.1016/j.dark.2018.11.002)
- Birrer, S., Shajib, A., Gilman, D., et al. 2021, The Journal of Open Source Software, 6, 3283, doi: [10.21105/joss.03283](https://doi.org/10.21105/joss.03283)
- Bradley, L., Sipőcz, B., Robitaille, T., et al. 2025, astropy/photutils: 2.2.0, 2.2.0 Zenodo, doi: [10.5281/zenodo.14889440](https://doi.org/10.5281/zenodo.14889440)
- Bradley, L. D., Coe, D., Brammer, G., et al. 2023, ApJ, 955, 13, doi: [10.3847/1538-4357/acecfe](https://doi.org/10.3847/1538-4357/acecfe)
- Brammer, G. 2023a, grizli, 1.9.11 Zenodo, doi: [10.5281/zenodo.1146904](https://doi.org/10.5281/zenodo.1146904)
- Brammer, G. 2023b, grizli, 1.9.11 Zenodo, doi: [10.5281/zenodo.8370018](https://doi.org/10.5281/zenodo.8370018)

- Burke, C. J., Stone, Z., Shen, Y., & Jiang, Y.-F. 2025, arXiv e-prints, arXiv:2511.16082, doi: [10.48550/arXiv.2511.16082](https://doi.org/10.48550/arXiv.2511.16082)
- Calzetti, D., Kinney, A. L., & Storchi-Bergmann, T. 1994, *ApJ*, 429, 582, doi: [10.1086/174346](https://doi.org/10.1086/174346)
- Carnall, A. C., McLure, R. J., Dunlop, J. S., & Davé, R. 2018, *MNRAS*, 480, 4379, doi: [10.1093/mnras/sty2169](https://doi.org/10.1093/mnras/sty2169)
- Chen, C.-H., Ho, L. C., Li, R., & Inayoshi, K. 2025a, *ApJL*, 989, L12, doi: [10.3847/2041-8213/adee0a](https://doi.org/10.3847/2041-8213/adee0a)
- Chen, C.-H., Ho, L. C., Li, R., & Zhuang, M.-Y. 2025b, *ApJ*, 983, 60, doi: [10.3847/1538-4357/ada93a](https://doi.org/10.3847/1538-4357/ada93a)
- Chen, X., Ichikawa, K., Akiyama, M., et al. 2025, arXiv e-prints, arXiv:2510.02801, doi: [10.48550/arXiv.2510.02801](https://doi.org/10.48550/arXiv.2510.02801)
- Clarke, L., Shapley, A. E., Sanders, R. L., et al. 2024, *ApJ*, 977, 133, doi: [10.3847/1538-4357/ad8ba4](https://doi.org/10.3847/1538-4357/ad8ba4)
- Coe, D., Salmon, B., Bradač, M., et al. 2019, *ApJ*, 884, 85, doi: [10.3847/1538-4357/ab412b](https://doi.org/10.3847/1538-4357/ab412b)
- de Graaff, A., Rix, H.-W., Naidu, R. P., et al. 2025a, *A&A*, 701, A168, doi: [10.1051/0004-6361/202554681](https://doi.org/10.1051/0004-6361/202554681)
- de Graaff, A., Hviding, R. E., Naidu, R. P., et al. 2025b, arXiv e-prints, arXiv:2511.21820, doi: [10.48550/arXiv.2511.21820](https://doi.org/10.48550/arXiv.2511.21820)
- Dekel, A., Stone, N. C., Chowdhury, D. D., et al. 2025, *A&A*, 695, A97, doi: [10.1051/0004-6361/202452393](https://doi.org/10.1051/0004-6361/202452393)
- Elíasdóttir, Á., Limousin, M., Richard, J., et al. 2007, arXiv e-prints, arXiv:0710.5636, doi: [10.48550/arXiv.0710.5636](https://doi.org/10.48550/arXiv.0710.5636)
- Endsley, R., Stark, D. P., Whitler, L., et al. 2024, *MNRAS*, 533, 1111, doi: [10.1093/mnras/stae1857](https://doi.org/10.1093/mnras/stae1857)
- Ferland, G. J., Korista, K. T., Verner, D. A., et al. 1998, *PASP*, 110, 761, doi: [10.1086/316190](https://doi.org/10.1086/316190)
- Finkelstein, S. L., Bagley, M. B., Arrabal Haro, P., et al. 2022, *ApJL*, 940, L55, doi: [10.3847/2041-8213/ac966e](https://doi.org/10.3847/2041-8213/ac966e)
- Fujii, M. S., Wang, L., Tanikawa, A., Hirai, Y., & Saitoh, T. R. 2024, *Science*, 384, 1488, doi: [10.1126/science.adi4211](https://doi.org/10.1126/science.adi4211)
- Furtak, L. J., Zitrin, A., Plat, A., et al. 2023a, *ApJ*, 952, 142, doi: [10.3847/1538-4357/acdc9d](https://doi.org/10.3847/1538-4357/acdc9d)
- Furtak, L. J., Zitrin, A., Weaver, J. R., et al. 2023b, *MNRAS*, 523, 4568, doi: [10.1093/mnras/stad1627](https://doi.org/10.1093/mnras/stad1627)
- Furtak, L. J., Labbé, I., Zitrin, A., et al. 2024, *Nature*, 628, 57, doi: [10.1038/s41586-024-07184-8](https://doi.org/10.1038/s41586-024-07184-8)
- Gloude-mans, A. J., Duncan, K. J., Eilers, A.-C., et al. 2025, *ApJ*, 986, 130, doi: [10.3847/1538-4357/adddb9](https://doi.org/10.3847/1538-4357/adddb9)
- Golubchik, M., Furtak, L. J., Allingham, J. F. V., et al. 2025, arXiv e-prints, arXiv:2512.02117, doi: [10.48550/arXiv.2512.02117](https://doi.org/10.48550/arXiv.2512.02117)
- Greene, J. E., Strader, J., & Ho, L. C. 2020, *ARA&A*, 58, 257, doi: [10.1146/annurev-astro-032620-021835](https://doi.org/10.1146/annurev-astro-032620-021835)
- Greene, J. E., Labbe, I., Goulding, A. D., et al. 2024, *ApJ*, 964, 39, doi: [10.3847/1538-4357/ad1e5f](https://doi.org/10.3847/1538-4357/ad1e5f)
- Greene, J. E., Setton, D. J., Furtak, L. J., et al. 2025, arXiv e-prints, arXiv:2509.05434, doi: [10.48550/arXiv.2509.05434](https://doi.org/10.48550/arXiv.2509.05434)
- Gunasekera, C. M., van Hoof, P. A. M., Chatzikos, M., & Ferland, G. J. 2023, *Research Notes of the American Astronomical Society*, 7, 246, doi: [10.3847/2515-5172/ad0e75](https://doi.org/10.3847/2515-5172/ad0e75)
- Harikane, Y., Zhang, Y., Nakajima, K., et al. 2023, *ApJ*, 959, 39, doi: [10.3847/1538-4357/ad029e](https://doi.org/10.3847/1538-4357/ad029e)
- Inayoshi, K. 2025, *ApJL*, 988, L22, doi: [10.3847/2041-8213/adea66](https://doi.org/10.3847/2041-8213/adea66)
- Inayoshi, K., & Ho, L. C. 2025, arXiv e-prints, arXiv:2512.03130, doi: [10.48550/arXiv.2512.03130](https://doi.org/10.48550/arXiv.2512.03130)
- Inayoshi, K., & Maiolino, R. 2025, *ApJL*, 980, L27, doi: [10.3847/2041-8213/adaebd](https://doi.org/10.3847/2041-8213/adaebd)
- Inayoshi, K., Murase, K., & Kashiyama, K. 2025, arXiv e-prints, arXiv:2509.19422, doi: [10.48550/arXiv.2509.19422](https://doi.org/10.48550/arXiv.2509.19422)
- Izotov, Y. I., & Thuan, T. X. 2008, *ApJ*, 687, 133, doi: [10.1086/591660](https://doi.org/10.1086/591660)
- Ji, X., Maiolino, R., Übler, H., et al. 2025, *MNRAS*, 544, 3900, doi: [10.1093/mnras/staf1867](https://doi.org/10.1093/mnras/staf1867)
- Keeton, C. R. 2001, arXiv e-prints, astro, doi: [10.48550/arXiv.astro-ph/0102341](https://doi.org/10.48550/arXiv.astro-ph/0102341)
- Kido, D., Ioka, K., Hotokezaka, K., Inayoshi, K., & Irwin, C. M. 2025, *MNRAS*, 544, 3407, doi: [10.1093/mnras/staf1898](https://doi.org/10.1093/mnras/staf1898)
- Killi, M., Watson, D., Brammer, G., et al. 2024, *A&A*, 691, A52, doi: [10.1051/0004-6361/202348857](https://doi.org/10.1051/0004-6361/202348857)
- Kocevski, D. D., Onoue, M., Inayoshi, K., et al. 2023, *ApJL*, 954, L4, doi: [10.3847/2041-8213/ace5a0](https://doi.org/10.3847/2041-8213/ace5a0)
- Kocevski, D. D., Finkelstein, S. L., Barro, G., et al. 2025, *ApJ*, 986, 126, doi: [10.3847/1538-4357/adbc7d](https://doi.org/10.3847/1538-4357/adbc7d)
- Kokorev, V., Brammer, G., Fujimoto, S., et al. 2022, *ApJS*, 263, 38, doi: [10.3847/1538-4365/ac9909](https://doi.org/10.3847/1538-4365/ac9909)
- Kokorev, V., Caputi, K. I., Greene, J. E., et al. 2024, *ApJ*, 968, 38, doi: [10.3847/1538-4357/ad4265](https://doi.org/10.3847/1538-4357/ad4265)
- Kokorev, V., Atek, H., Chisholm, J., et al. 2025, *ApJL*, 983, L22, doi: [10.3847/2041-8213/adc458](https://doi.org/10.3847/2041-8213/adc458)
- Kokubo, M., & Harikane, Y. 2025, *ApJ*, 995, 24, doi: [10.3847/1538-4357/ae119e](https://doi.org/10.3847/1538-4357/ae119e)
- Labbe, I., Greene, J. E., Bezanson, R., et al. 2025, *ApJ*, 978, 92, doi: [10.3847/1538-4357/ad3551](https://doi.org/10.3847/1538-4357/ad3551)
- Lin, R., Zheng, Z.-Y., Jiang, C., et al. 2025, *ApJL*, 980, L34, doi: [10.3847/2041-8213/adaaf1](https://doi.org/10.3847/2041-8213/adaaf1)
- Lin, X., Fan, X., Cai, Z., et al. 2025, arXiv e-prints, arXiv:2507.10659, doi: [10.48550/arXiv.2507.10659](https://doi.org/10.48550/arXiv.2507.10659)

- Maiolino, R., Risaliti, G., Signorini, M., et al. 2025, MNRAS, 538, 1921, doi: [10.1093/mnras/staf359](https://doi.org/10.1093/mnras/staf359)
- Matthee, J., Naidu, R. P., Brammer, G., et al. 2024, ApJ, 963, 129, doi: [10.3847/1538-4357/ad2345](https://doi.org/10.3847/1538-4357/ad2345)
- Mérida, R. M., Gaspar, G., Sawicki, M., et al. 2025, A&A, 698, A317, doi: [10.1051/0004-6361/202553943](https://doi.org/10.1051/0004-6361/202553943)
- Miller, T. B., Suess, K. A., Setton, D. J., et al. 2025, ApJ, 988, 196, doi: [10.3847/1538-4357/ade438](https://doi.org/10.3847/1538-4357/ade438)
- Morishita, T., Stiavelli, M., Chary, R.-R., et al. 2024, ApJ, 963, 9, doi: [10.3847/1538-4357/ad1404](https://doi.org/10.3847/1538-4357/ad1404)
- Naidu, R. P., Matthee, J., Katz, H., et al. 2025, arXiv e-prints, arXiv:2503.16596, doi: [10.48550/arXiv.2503.16596](https://doi.org/10.48550/arXiv.2503.16596)
- Oke, J. B., & Gunn, J. E. 1983, ApJ, 266, 713, doi: [10.1086/160817](https://doi.org/10.1086/160817)
- Ono, Y., Ouchi, M., Harikane, Y., et al. 2025, ApJ, 991, 222, doi: [10.3847/1538-4357/adfc4d](https://doi.org/10.3847/1538-4357/adfc4d)
- Pascale, M., Frye, B. L., Dai, L., et al. 2022, ApJ, 932, 85, doi: [10.3847/1538-4357/ac6ce9](https://doi.org/10.3847/1538-4357/ac6ce9)
- Planck Collaboration, Aghanim, N., Akrami, Y., et al. 2020, A&A, 641, A6, doi: [10.1051/0004-6361/201833910](https://doi.org/10.1051/0004-6361/201833910)
- Portegies Zwart, S. F., Baumgardt, H., Hut, P., Makino, J., & McMillan, S. L. W. 2004, Nature, 428, 724, doi: [10.1038/nature02448](https://doi.org/10.1038/nature02448)
- Portegies Zwart, S. F., & McMillan, S. L. W. 2002, ApJ, 576, 899, doi: [10.1086/341798](https://doi.org/10.1086/341798)
- Rigby, J., Perrin, M., McElwain, M., et al. 2023, PASP, 135, 048001, doi: [10.1088/1538-3873/acb293](https://doi.org/10.1088/1538-3873/acb293)
- Rinaldi, P., Bonaventura, N., Rieke, G. H., et al. 2025, ApJ, 992, 71, doi: [10.3847/1538-4357/adfa10](https://doi.org/10.3847/1538-4357/adfa10)
- Ronayne, K., Papovich, C., Kirkpatrick, A., et al. 2025, arXiv e-prints, arXiv:2508.20177, doi: [10.48550/arXiv.2508.20177](https://doi.org/10.48550/arXiv.2508.20177)
- Sakurai, Y., Yoshida, N., Fujii, M. S., & Hirano, S. 2017, MNRAS, 472, 1677, doi: [10.1093/mnras/stx2044](https://doi.org/10.1093/mnras/stx2044)
- Salmon, B., Coe, D., Bradley, L., et al. 2020, ApJ, 889, 189, doi: [10.3847/1538-4357/ab5a8b](https://doi.org/10.3847/1538-4357/ab5a8b)
- Shibuya, T., Ouchi, M., Harikane, Y., & Nakajima, K. 2019, ApJ, 871, 164, doi: [10.3847/1538-4357/aaf64b](https://doi.org/10.3847/1538-4357/aaf64b)
- Sifón, C., Menanteau, F., Hughes, J. P., Carrasco, M., & Barrientos, L. F. 2014, A&A, 562, A43, doi: [10.1051/0004-6361/201321638](https://doi.org/10.1051/0004-6361/201321638)
- Stanway, E. R., & Eldridge, J. J. 2018, MNRAS, 479, 75, doi: [10.1093/mnras/sty1353](https://doi.org/10.1093/mnras/sty1353)
- Stone, Z., Shen, Y., Zhuang, M.-Y., et al. 2025, arXiv e-prints, arXiv:2509.19585, doi: [10.48550/arXiv.2509.19585](https://doi.org/10.48550/arXiv.2509.19585)
- Tanaka, T. S., Silverman, J. D., Shimasaku, K., et al. 2024, arXiv e-prints, arXiv:2412.14246, doi: [10.48550/arXiv.2412.14246](https://doi.org/10.48550/arXiv.2412.14246)
- Tanaka, T. S., Akins, H. B., Harikane, Y., et al. 2025, ApJ, 995, 21, doi: [10.3847/1538-4357/ae145f](https://doi.org/10.3847/1538-4357/ae145f)
- Tarrío, P., Melin, J.-B., & Arnaud, M. 2019, A&A, 626, A7, doi: [10.1051/0004-6361/201834979](https://doi.org/10.1051/0004-6361/201834979)
- Tee, W. L., Fan, X., Wang, F., & Yang, J. 2025, ApJL, 983, L26, doi: [10.3847/2041-8213/adc5e3](https://doi.org/10.3847/2041-8213/adc5e3)
- Übler, H., Mazzolari, G., Maiolino, R., et al. 2025, arXiv e-prints, arXiv:2509.21575, doi: [10.48550/arXiv.2509.21575](https://doi.org/10.48550/arXiv.2509.21575)
- Umeda, H., Inayoshi, K., Harikane, Y., & Murase, K. 2025, arXiv e-prints, arXiv:2512.04208, doi: [10.48550/arXiv.2512.04208](https://doi.org/10.48550/arXiv.2512.04208)
- Williams, C. C., Alberts, S., Ji, Z., et al. 2024, ApJ, 968, 34, doi: [10.3847/1538-4357/ad3f17](https://doi.org/10.3847/1538-4357/ad3f17)
- Yang, L., Birrer, S., & Treu, T. 2020, MNRAS, 496, 2648, doi: [10.1093/mnras/staa1649](https://doi.org/10.1093/mnras/staa1649)
- Yue, M., Eilers, A.-C., Ananna, T. T., et al. 2024, ApJL, 974, L26, doi: [10.3847/2041-8213/ad7eba](https://doi.org/10.3847/2041-8213/ad7eba)
- Zhang, S., Liu, B., & Bromm, V. 2025, ApJ, 992, 136, doi: [10.3847/1538-4357/ae061c](https://doi.org/10.3847/1538-4357/ae061c)
- Zhang, Y., Ding, X., Yang, L., et al. 2025, arXiv e-prints, arXiv:2510.25830, doi: [10.48550/arXiv.2510.25830](https://doi.org/10.48550/arXiv.2510.25830)
- Zhang, Z., Jiang, L., Liu, W., & Ho, L. C. 2025a, ApJ, 985, 119, doi: [10.3847/1538-4357/adcb3e](https://doi.org/10.3847/1538-4357/adcb3e)
- Zhang, Z., Li, M., Oguri, M., et al. 2025b, arXiv e-prints, arXiv:2512.05180, doi: [10.48550/arXiv.2512.05180](https://doi.org/10.48550/arXiv.2512.05180)
- Zitrin, A., Fabris, A., Merten, J., et al. 2015, ApJ, 801, 44, doi: [10.1088/0004-637X/801/1/44](https://doi.org/10.1088/0004-637X/801/1/44)